Pak. J. Biochem. Mol. Biol., 2024, 57(3):62-85

Research Paper

Homology modeling and ligand docking of human brain-derived neurotrophic factor (*BDNF)*

Ibtsam Bilal[1], Kainat Ramzan[1*], Saira Ramzan[3], Moeen Zulfiqar[2], Usama Tahir[1], Ali Moazzam[2], and Imran Haider[1]

[1]Department of Biochemistry, University of Okara, Okara, Pakistan. [2]Department of Molecular Biology, University of Okara, Okara, Pakistan. [3]Department of Zoology, University of Okara, Okara, Pakistan.

***Corresponding author**: Kainat Ramzan, kainatramzan54@gmail.com

ABSTRACT

Brain-derived neurotrophic factor, a protein belonging to the neurotrophin family, interacts with receptors known as TrkB and p75NTR that are present in the nervous system. A *BDNF* gene is responsible for the plasticity of glutamate, and GABA synapses and also influences the differentiation of neurons and impacts serotonergic and dopaminergic neurotransmission. The present study presents strcuctural bioinformatics of the *BDNF* protein, assessing structural and functional consequences by predicting its sequence analysis and structural modeling. The results found that *BDNF* is negatively charged, and non-polar with a hydrophilic and soluble GRAVY score of -0.456 and is generally unstable, based on its physiochemical attributes. The prevalence of α-helices relative to β-type structures highlights significant structural characteristics associated with the functional *BDNF* elements. The selected protein was studied using in-silico tools for 3D structure prediction as a potential target for protein-ligand docking analysis. PyRx tool findings revealed that IND24, Congo red, Neoamphimedine, Amphimedine, Deoxyamphimedine, and Emetine had the highest docking scores and the most stable interactions with the protein model. Based on these findings, the selected protein emerges as a promising target for protein-ligand docking, a computational method for identifying potential drug molecules. Through protein-ligand docking, researchers aim to discover new therapeutic candidates that can modulate the function of the selected protein and potentially impact associated brain diseases.

Keywords: *BDNF*, TrkB, p75NTR, GABAergic, GWAS

INTRODUCTION

Single nucleotide variants (SNVs) play a crucial role in the genetic differences observed among humans, accounting for approximately 90% of these variations. They occur when there is a change in a single base pair within alleles, resulting in distinct differences in the genome sequence (1-3). Most mutations in human DNA are attributed to single nucleotide polymorphisms (SNPs), which significantly influence gene phenotypes and tumor exposure (4, 5). Roughly 0.5 million SNPs are found in the coding region of human DNA which impairs the stability and synthesis of proteins (6). Extensive research is important to comprehend the various genetic variants' relevance and consequences (7). Nowadays, computational biology and bioinformatics have led to innovations that function effectively with molecular biology interfaces (8) and raised the importance of the protein folding challenge in contemporary biology (9, 10). Notably, abnormal brain-derived neurotrophic factor (*BDNF)* levels are linked to the development of anxiety, drug dependence, obsessional disorder, and mental diseases, all are hallmarks of neuropsychiatric conditions (11).

In developed economies, over 50% of people will experience at least one psychological disorder in their lifetime. Moreover, it is estimated that the economic cost of psychiatric disorders will be around $16.3 million between 2011 and 2030, surpassing the costs of diabetes, cancer, and respiratory disorders and exceeding the expense of cardiac failure (12). Various neuropsychiatric disorders have been linked to regulating the *BDNF* gene and the protein profile

of leukocytes derived from the bloodstream (13). The identification of genetic polymorphisms in the *BDNF* gene has been linked to deregulation of gene expression and disruptions in cellular signaling (14, 15). Notably, missense *BDNF* mutations are known to affect both neuronal and dendritic structures, resulting in abnormal development and premature dendritic growth (16). Nearly, 1768 missense variants have been identified and the most commonly observed SNP (rs6265) replaces valine with methionine at position 66. The rs6265 variant has been associated with a reduction in *BDNF* production and is linked with cognitive impairments in multiple studies (17-20).

The neural growth factor (NGF) family of proteins is encoded by the *BDNF* gene, also known by alternative names such as Abrineurin, *ANON2*, and *BULN2*. It exhibits high expression levels within the nervous system and plays a crucial role in various biological functions associated with brain growth and development by interacting with tropomyosin receptor kinase B (TrkB) (21, 22). The primary producers of *BDNF* protein are microglia, astrocytes in the cortex and hippocampus, and glutamatergic neurons (23-25). The peripheral and white adipose tissue both respond to the synthesis of *BDNF* in the presence of metabolic stress (26, 27). The *BDNF* and TrkB receptors are prevalent in the amygdala and cortical lobes of neurons. Although *BDNF*'s effects on the brain have been extensively studied, their biological significance in various organs remains unclear (28, 29).

Since *BDNF* is involved in neural plasticity, neurogenesis, and prolonged potentiation, reduced *BDNF* expression is linked to Huntington's disease, Alzheimer's disease, schizophrenia, and bipolar disorder (30, 31). By affecting pre- and post-synaptic regions, the *BDNF* is believed to alter synaptic efficiency and cause long-lasting changes in synaptic plasticity (32-34). Furthermore, it can modify serotonergic and dopaminergic nerve signals by altering brain plasticity. Epidemiological studies showed that impaired glucose metabolism is often linked to reduced *BDNF*, which may be associated with dementia, anxiety, and type 2 diabetes (35). Research revealed that peripheral delivery of *BDNF* causes hyperphagic and hypoglycemic effects in obese hyperglycemic mice, highlighting its possible anti-obesity and anti-diabetic properties (36).

The *BDNF* protein was identified in 1982 that encodes a secretory protein with 247 amino acid residues (37) and mapped on a human chromosome 11p14.1. It comprises a region from 27654892 to 27722057 base pairs (38). There are 11 exons and several *BDNF* isoforms that result from the use of alternative regulators and spliced functions (13, 39). The neurotrophin family comprises genes such as NGF, neurotrophin-3 (NT-3), neurotrophin-4 (NT-4), and NT-6 which is different from the other members (40). An early protein known as pro-*BDNF* originates in the endoplasmic reticulum (ER). The Golgi apparatus and trans-Golgi networks produce pro-*BDNF*(32–35 kDa) (41-43). A form of biologically mature *BDNF* (13 kDa) protein can result from the subsequent cleavage of pro-*BDNF* by certain protein convertase enzymes (matrix metalloproteases) in the trans-Golgi network (44), then mBDNF is produced as a dimer made up of two proteins that are not covalently bonded (45). Dimeric pro- and m-*BDNF* can be secreted by cells, and granular deposition is enabled by activity-dependent exocytosis (46). The binding of such homodimers to specific receptors (such as Trka and p75NTR) was shown to initiate multiple cellular signaling pathways that involved neuronal growth, development, and stability (47, 48). Using diverse splicing mechanisms, scientists found 17 unique transcripts of mRNA for the human *BDNF* gene (49).

The PI3K, MAPK/ERK, and PLCg pathways of intracellular signaling are linked to both *BDNF* and TrkB (15, 50). It shares 50% protein sequence overlap with NT-3, NT-4/5, and NGF, and retains structural similarities. Each neurotrophin is composed of an indirectly linked homodimer with an N-linked glycosylation site in the pro-region and a signal peptide after the initiation codon (41-43). Understanding the crystal structures of proteins is crucial to comprehending their biological functions and the potential structural changes caused by mutations associated with diseases (51, 52). Traditionally,

protein 3D structures have been determined by labor-intensive and cost-effective methods including nuclear magnetic resonance (NMR) and the X-ray diffraction pattern. Consequently, there is a substantial gap between the number of significantly proven structures and multiple gene sequences produced with rapid and affordable sequencing methods (52, 53). To solve such challenges, computational methods are increasingly being used to predict protein structures and identify the probability of genetic mutations (52, 54). The present study examines the physiochemical properties of *BDNF* proteins and offers predictions about their structural composition by using bioinformatic tools. Based on homology modeling and protein-ligand docking analyses, it appears that the identified protein may be effectively used as the desired target in further experimental research. This knowledge will be useful in confirming the anticipated interactions and exploring any potential therapeutic effects. To fully comprehend their role and potential treatment implications in diseases, more research is required.

MATERIALS AND METHODS

Download query sequence

The *BDNF* gene sequence and its protein reference sequence are derived from the National Center for Biotechnology Information (NCBI) [http://www.ncbi.nlm.nih.gov] and UniProt databases [https://www.uniprot.org], respectively (55, 56). A protein sequence generated by the aforementioned data was then used for further computational study and (Figure1) depicts the study design schematically.

Physiochemical characterization of *BDNF* protein

Protparam tool [web.expasy.org/protparam] was employed to access the physiochemical attributes of human *BDNF* protein (57). This tool utilizes the Edelhoch method to calculate values such as the weight of instability concerning 400 different dipeptides (DIWV), and also the composition of the protein sequence. Furthermore, the instability index (II), aliphatic index (AI), and GRAVY which assesses the sequence hydrophobicity/hydrophilicity, and extinction coefficients were examined by ExPASy ProtParam server (58, 59).

Protein secondary structure prediction

The Self-Optimized Prediction method With Alignment tool [SOPMA: https://npsa-prabi.ibcp.fr/cgi-bin/npsa_automat.pl?page=/NPSA/npsa_sopma.html] used to predict the secondary structure of proteins. When SOPMA is combined with the neural network method PHD, it can accurately predict 82.2% of residues for 74% of co-predicted amino acids (60, 61). Additionally, the PSI-blast-based secondary structure prediction method (PSIPRED) server [http://bioinf.cs.ucl.ac.uk/psipred] was also employed to assess the secondary structure of the protein (62). Both tools accept a FASTA format as input and develop secondary protein structure prediction by comprising αlpha-helix, βeta-sheet, and turn components anticipated. These forecasts are acute for comprehending the folding and structural properties of the *BDNF* protein (63-66).

Predicting the Protein-protein interactions

Protein-protein interactions (PPI) are known to have a significant impact on numerous biological processes. The Search Tool for the Retrieval of Interacting Genes/Proteins database [STRING: https://string-db.org] tool has been employed for evaluating interactions between reported proteins (67). It combines data from physical interaction databases and curated biological pathway knowledge to offer a comprehensive assessment of protein-protein interactions. The input was the protein sequence, and the results provided important insights into the interactions involving the *BDNF* protein (68, 69).

Secondly, GeneMANIA [www.genemania.org] is employed to examine protein work by combining proteomics and genomics datasets of unknown proteins (70). The resulting graphic depicts the physical interactions between the target and its related genes. This image provides a visual representation of the relationships and interactions within the network, aiding in the

understanding of *BDNF's* role and its correlated genes in biological processes (63).

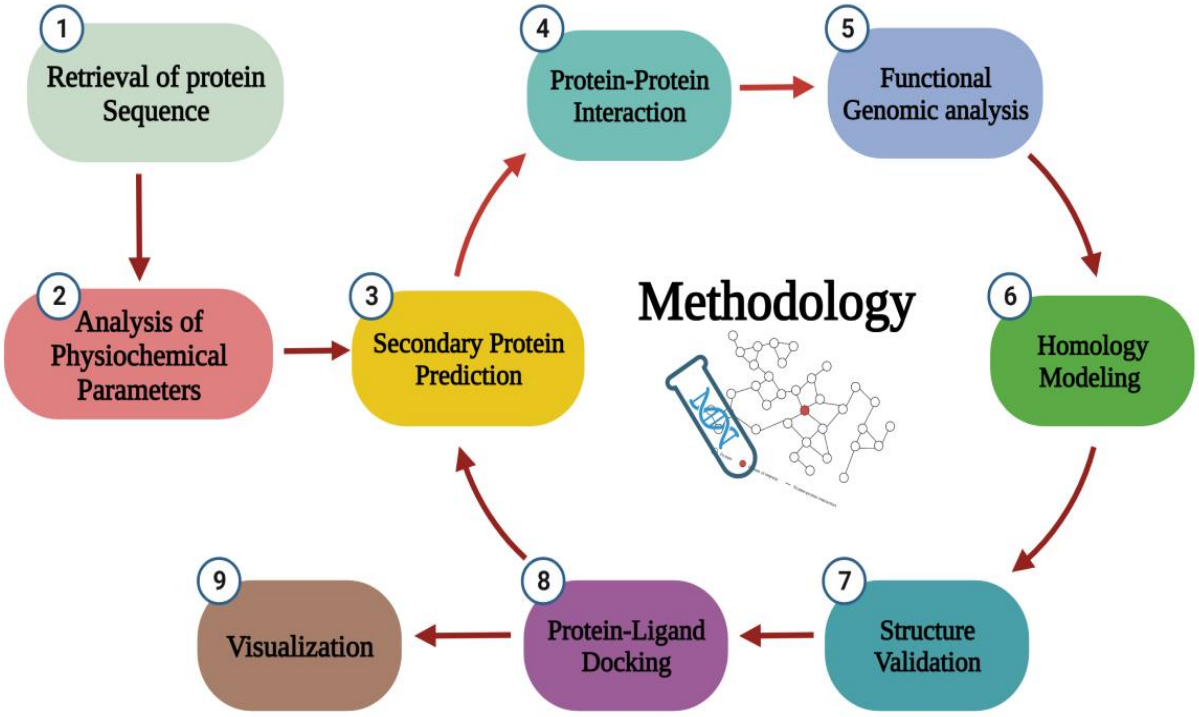

Figure 1 Diagrammatic representation of the general concept utilized in the current study.

Tertairy structure prediction

To forecast the 3-dimensional (3D) structure, homology modeling was performed since no crystal structure was fully available. Several bioinformatic programs were used, including the Swiss model (71), Modeller 10.3(72), HHPred (73), and i-TASSER (74), which employ threading and template identification methods to generate accurate 3D models. HHpred [http://toolkit.tuebingen.mpg.de/hhpred] utilizes multiple sequence alignments of related sequences, often obtained through the PSI-BLAST program, to calculate HHPred profiles and serve for predicting protein 3D structures. The template structures for *BDNF* modeling were obtained by submitting the FASTA sequence, then it was compared to a database of known protein structures to assess the suitable templates with structural similarities (75-77).

Moreover, MODELLER 10.3 [https://salilab.org/modeller/download_installation.html], a software tool used for comparative protein modeling. A total of ten models were generated, and the selection of the best model was based on criteria such as the objective function score and DOPE value (72, 78-80). The SWISS-MODEL [https://swissmodel.expasy.org], a fully automated homology-modeling server, was employed to forecast the crystal structure of a target protein (81). To start the modeling process, the FASTA format sequence was submitted as input (82). The Iterative Threading ASSEmbly Refinement [https://zhanggroup.org/I-TASSER] server is highly regarded for its accuracy and employs the PDB template database to identify appropriate structural templates (63, 83). This provides the top 5 models for the targeted protein, the input for the I-TASSER server was the protein FASTA sequence (83, 84). To visualize the 3D structures, software tools such as UCSF Chimera [https://www.cgl.ucsf.edu/chimera](85), Discovery Studio [https://discover.3ds.com/discovery-studio-visualizer] [84],

and PyMOL [https://pymol.org] was employed (86).

Structure Analysis

To evaluate the accuracy of the selected protein models, the SAVES Server [https://saves.mbi.ucla.edu] was employed, by incorporating the PROCHECK, 3D Verify, and ERRAT modules (74, 87). ERRAT evaluates the overall efficacy of the model by assessing the probability distribution of non-bonded associations among a variety of atoms based on unique atomic correlations. On Verify, a score exceeding 80% indicates that the quality of a predicted model is good (56, 74). ProCHECK-RAMACHANDRAN plot calculates the stereochemical geometry (phi (φ)-psi (ψ) angles) of a target protein. This plot depicts the conformations of residues in allowed and forbidden regions, with over 90% of residue in most preferred zones indicating high quality (78).

The model quality was evaluated using the Qualitative Model Energy Analysis (QMEAN) server [https://swissmodel.expasy.org/qmean] by analyzing various geometrical properties (88). The ProSA tool [https://prosa.services.came.sbg.ac.at/prosa.php] is used to distinguish potential errors in the protein model by evaluating its atomic coordinates. This tool identifies erroneous structures based on Z-scores that exceed the typical range observed in native proteins. High Z-scores indicate potential issues such as incorrect folding or structural abnormalities, guiding researchers in identifying and correcting errors in the protein model (89, 90).

Screening of Ligands (small compounds)

The Structure Data File (SDF) files of the identified ligands were obtained from PubChem [https://pubchem.ncbi.nlm.nih.gov], and the ZINC databank [https://zinc.docking.org]. Relevant literature was reviewed to obtain data on these compounds and their biological characteristics. The SDF files of the ligand structures were converted to the PDB format using the PyMOL program[https://pymol.org/2]. The resulting conversion made it possible to analyze and modify the ligand structures in an acceptable format (86).

Protein-Ligand docking analysis

With the completion of the Human Genome Project (HGP), the range of biological targets available for use in therapeutic research was increased. Recent methods including NMR analysis, protein extraction, and high-throughput crystallography yield information on complex and protein-ligand interactions (91, 92). Such advances have made it possible to use automated drug design approaches, particularly molecular docking methods (93) to identify the most potent inhibitor for drug designing to treat *BDNF*-related disorders (94). Different algorithms such as Glide, Gold, AutoDock, PyRx, Surflex, ICM, FITTED, and Molecular Operating Environment (MOE) were developed for protein-ligand docking, with an emphasis on finding drugs based on structured small molecules (95).

In this study, the ligands were docked with the derived 3D protein structure using the PyRx tool [https://pyrx.sourceforge.io], which includes AutoDock and AutoDock Vina, to discover the *BDNF* inhibitors. The criterion for virtual ligand screening was the Lamarckian genetic algorithm (LGA) (96-98). The 10 most distinct conformations for each ligand were computed throughout the docking process, which used defined parameters such as the grid size at the center (XYZ axis). AutoDock programs were utilized to convert the PDB files of the proteins and ligands into the PDBQT format (99). The docking results were visualized and analyzed in both 2D and 3D representations using the DS Visualizer (100).

Results

Identification of the *BDNF* sequence

The human *BDNF* protein (P23560) has a 247 amino acid sequence that can be found in the UniProt databases. The 3D structure of the *BDNF* protein was modeled using the aforementioned sequence as an input. Table 1 summarizes key properties of the *BDNF* protein obtained from the NCBI database, including its gene name, length, exon composition, UniProt number, data source, and sequence information.

Table 1: Retrieval of primary *BDNF* protein information

Protein Individualities	Protein Information
Recommended Name	Brain-derived neurotrophic factor (*BDNF*)
Amino Acids	247
Gene ID	627
Ensembl ID	ENSG00000176697
Location	11p14.1
Exon count	12
NCBI Nucleotide	NC_000011.10
Base Pairs	27654893-27722030
Primary accession	P23560
Organism	*Homo Sapiens*
FASTA sequence	>NP_001700.2 brain-derived neurotrophic factor isoform a preproprotein [Homo sapiens] MTILFLTMVISYFGCMKAAPMKEANIRGQGGLAYPGVRTHGTLESVNGPKAGSR GLTSLADTFEHVIEELLDEDQKVRPNEENNKDADLYTSRVMLSSQVPLEPPLLFL LEEYKNYLDAANMSMRVRRHSDPARRGELSVCDSISEWVTAADKKTAVDMSG GTVTVLEKVPVSKGQLKQYFYETKCNPMGYTKEGCRGIDKRHWNSQCRTTQSY VRALTMDSKKRIGWRFIRIDTSCVCTLTIKRGR

Characterization of physicochemical properties

The *BDNF* FASTA sequence was inputted into the ProtParam tool as the query sequence. Variables from Expasy's ProtParam were used to assess the physicochemical properties, as detailed in Table 2. The *BDNF* protein (P23560) consists of 247 amino acids, has a molecular weight of 27,817.94 daltons, and has a molecular formula of $C_{1211}H_{1950}N_{348}O_{368}S_{17}$. The P23560 contains 36 positively charged amino acids (arginine and lysine) and 29 negatively charged residues (aspartic acid and glutamic acid). The total number of atoms is estimated to be 3,894. The P23560 has an isoelectric point (pI) of 9.01, indicating its basic nature since the pI is above 7. The amino acid composition of the *BDNF* protein**.** The target protein has an aliphatic index of 74.57 and an instability index (II) of 43.34, indicating that it is unstable since values below 40 typically suggest stability.

Moreover, *BDNF*_HUMAN (P23560) has an extinction coefficient of 30,285 $M^{-1}cm^{-1}$, which measures the amount of light absorbed by the protein at 280 nm. The half-life, which refers to the time required for the protein concentration to decrease to half of its initial amount, was evaluated in yeast, human, and Escherichia coli cells, resulting in 30 hours, 20 hours, and 10 hours, respectively. With methionine as the N-terminal residue, the half-lives in mammalian reticulocytes (in vitro), yeast (in vivo), and *E. coli* (in vivo) are 30 hours, over 20 hours, and over 10 hours, respectively. Methionine as the N-terminal residue reduces the protein's half-life in *E. coli*. This protein is a negatively charged, non-polar, and relatively unstable protein. Its Grand Average of Hydropathy (GRAVY) index is -0.456, indicating that it is hydrophilic and soluble, with a low GRAVY index suggesting better interaction and higher solubility in water, as shown in Table 2.

Table 2: Physicochemical parameters by Protparam analysis

Properties	Values
Number of amino acids	247
Molecular Mass (MM)	27817.94
Theoretical point (pI)	9.01
Total number of negatively charged residues (Asp + Glu)	29

Total number of positively charged residues (Arg + Lys)	36
Formula	$C_{1211}H_{1950}N_{348}O_{368}S_{17}$
Total number of atoms	3894
Extinction coefficients	**1**. Ext. coefficient 30285; Abs 0.1% (=1 g/l) 1.089, assuming all pairs of Cys residues form cystines. **2**. Ext. coefficient 29910; Abs 0.1% (=1 g/l) 1.075, assuming all Cys residues are reduced
Estimated half-life	**a)** 30 hours (mammalian reticulocytes, in vitro), **b)** >20 hours (yeast, in vivo), **c)** >10 hours (Escherichia coli, in vivo).
Instability index	43.34
Aliphatic index	74.57
Grand average of hydropathicity (GRAVY)	-0.456

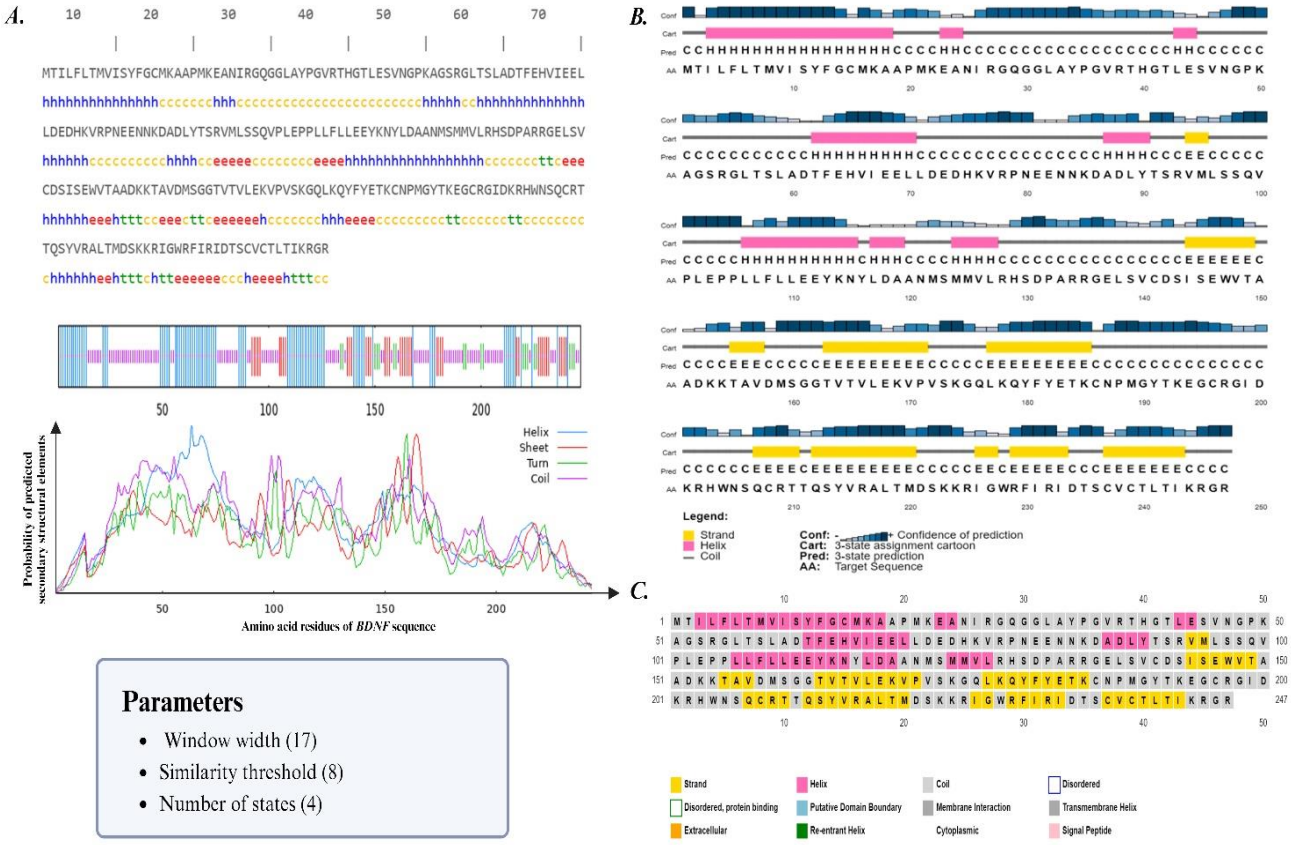

Figure 2: A) Secondary structure of *BDNF* amino acid residues as identified by SOPMA analysis. B) PSIPRED predicted the *BDNF* secondary structural elements for each residue in a cartoon depiction. C) A standard PSIPRED web server result webpage. Based on the anticipated SS class, each AA is classified and colored.

Modeling the secondary structure of *BDNF* protein

The interactions, arrangement, and efficiency of proteins are all strongly interconnected and rely on structural elements such as helix, coil, sheet,

and rotation [55–58]. The SOPMA analysis highlights the presence of secondary structure elements of *BDNF* protein (Figure 2A). The results of *BDNF* protein are summarized in Table 3, showing the percentages of α-helix (Hh), extended strands (Ee), β-turns (Tt), and random coils (Cc). Precisely, α-helices were predominant, comprising 34.82% (86 residues), extended strands accounted for 16.19% (40 residues), β-turns represented 7.69% (19 residues), and random coils made up the majority at 41.30% (102 residues). The significant amount of α-helices suggests inherent structural stability and strong thermal endurance of the *BDNF* protein. The prevalence of α-helices over β-type structures determines the crucial structural characteristics relevant to its functional properties. Moreover, the PSIPRED program provided confident predictions of 8 alpha helices, 10 strands, and coils in the *BDNF* protein (Figure 2B). A typical result page from the PSIPRED web server (Figure 2C), where all amino acids are listed and colored according to the predicted secondary structure class. This comprehensive study underscores the secondary structural characteristics of *BDNF* and offers valuable information on its stability and biological functions.

Table 3: Description of *BDNF* secondary structural elements by SOPMA server

Secondary Structure Elements	Values (%)
Alpha helix	86(34.82%)
310 helix	0.00%
Pi helix	0.00%
Beta bridge (Bb)	0.00%
Extended strand (Ee)	40 (16.19%)
Beta turn (Tt)	19 (7.69%)
Bend region (Ss)	0.00%
Random coil (Cc)	102 (41.30%)
Ambiguous states	0.00%
Other states	0.00%
Window width	17
Similarity threshold	8
Number of states	4

Homology modeling and structural analysis

The *BDNF* FASTA sequence was submitted to the HHPred tool, which produced a 100% likelihood for the ideal template (6XUO_A). With 170 aligned columns and an E-value of 4e-45 (107aa), this template met its desired length of 224 efficiently. The final 3D protein structure is displayed by Chimera and saved in PDB format (Figure 3). In addition, i-TASSER generated the top 10 structural analogs from the PDB to act as models for the modeling technique. The Z-score for the template with the highest score (PDB ID: 3bukA) was 2.33 compared to the human *BDNF* query sequence. It yielded five models for the target protein, of which MODEL 1 was selected based on its intriguing stereochemical properties and C-score (-3.22). The results of MODELLER 10.3 projected that MODEL 10 (bdnf.B99990010.pdb) would have a molpdf value of 1741.13892 and a GA341 score of 0.99899. Moreover, SWISS-MODEL used the best-aligned template from the Uniprot proteome to build 37 incomplete structures of the target protein that have a high degree of similarity with a query sequence. The *BDNF* structures (Figure 3) were produced using four homology modeling servers; HHPred, i-Tasser, modeller 10.3, and Swiss Model.

From SWISS Modeling, a template (Q4L0Y3.1.A) represents the crystal structure of a mutant *Spermophilus citellus* protein was selected. There was a 97.98% similarity between the query sequence and this template that covers the range 1-247 aa. Based on its oligomeric state, the predicted protein model was determined to be a monomer and uploaded in PDB format to the SAVES servers for quality evaluation. The findings showed that model number 2 (Q4L0Y3.1.A) was the most favorable, as defined in Table 4 that achieved a score of 90.8046% from ERRAT, the SWISS-MODEL evaluation revealed a RAMACHANDRAN core region of 90.30%. The Ramachandran plot produced by PROCHECK was used to evaluate the 3D structure of the *BDNF* protein, and Table 5 shows the statistics for the simulated protein.

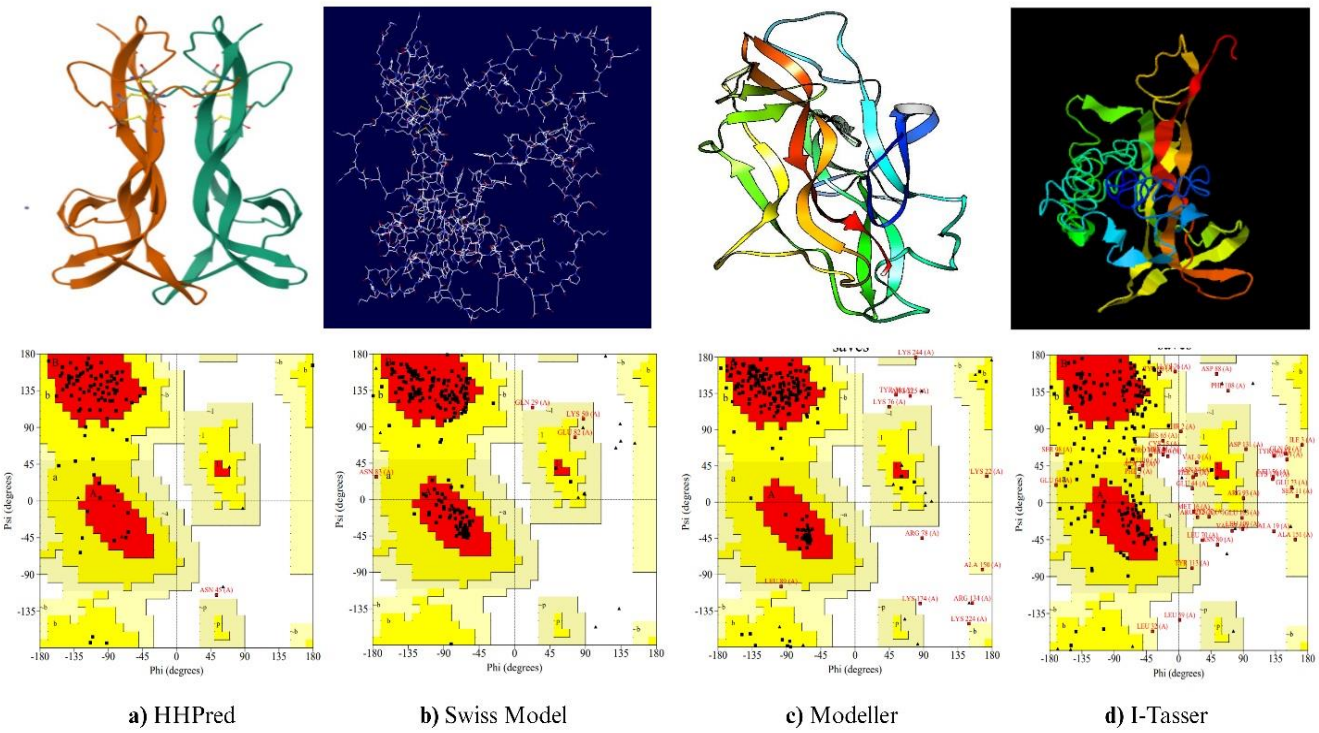

Figure 3: Protein modeling by using different algorithms a) HHPred b) Swiss Model c) Modeller d) I-Tasser

The provided data highlights the evaluation metrics of different *BDNF* prediction models. HHPred (6XUO_A) exhibits a QMEAN value of -0.77, a ProSA web Z-score of -5.75, and an ERRAT value of 95.699. The Swiss model (Q4L0Y3.1.A) shows a QMEAN value of -2.00, a ProSA web Z-score of -4.96, and an ERRAT value of 90.805. I-TASSER (model 1) has a QMEAN value of -3.09, a ProSA web Z-score of -1.96, and an ERRAT value of 82.077. Modeller 10.3 (bdnf.B99990010) demonstrates a QMEAN value of -6.20, a ProSA web Z-score of -3.23, and an ERRAT value of 34.310. These metrics are crucial for assessing the quality and reliability of selected structure predictions. The QMEAN values reflect the overall model quality, with the *BDNF* model represented as a red star (Figure 4A). The Verify 3D analysis of the simulated protein confirms that the average 3D-1D score for all amino acid residues is greater than 0.2, which is favorable for the estimated protein configuration (Figure 4B). The ProSA web Z-scores indicate the model's compatibility with experimental data (Figure 4C), and the ERRAT values assess the model's overall structural quality and accuracy, as detailed in Table 4.

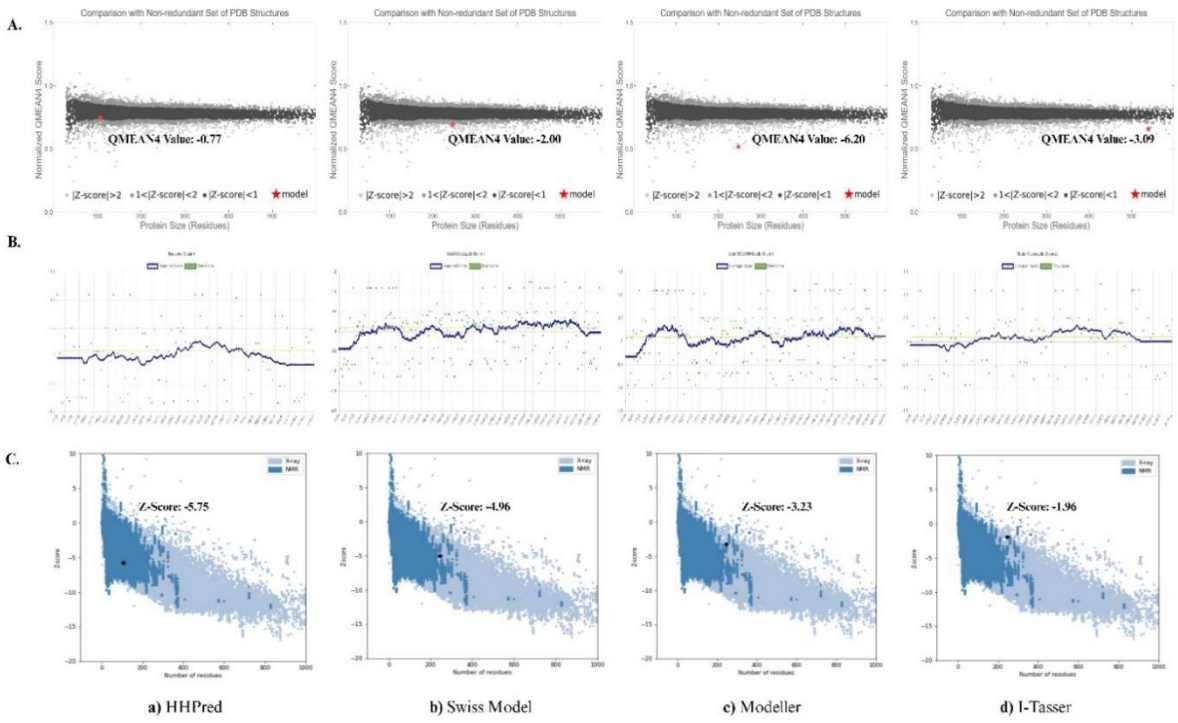

Figure 4: Modeled quality assessment by A) QMEAN B) Verify 3D C) ProSA web servers

Table 4: Structural validation by the SAVES server

	ERRAT	ProCheck				Verify 3D
Protein Templates	**Score**	**Core**	**Allow**	**Generously**	**Disallowed**	**Score**
HHPred (6XUO)	95.6989	83.50%	15.50%	0.00%	1.00%	23.36%
Q4L0Y3.1.A	90.8046	90.30%	7.80%	1.40%	0.50%	38.46%
Modeller (bdnf.B99990010)	34.310	83.40%	13.40%	2.30%	0.90%	61.13%
I-Tasser	82.0774	44.20%	36.90%	11.50%	7.40%	69.23%

Table 5: Statistics of the modeled *BDNF* proteins are displayed by the RAMACHANDRAN plot

Plot Statistics	6XUO	Q4L0Y3.1	bdnf.B99990010	3BUK
Residues in the most favored regions (A, B, L)	81 (83.5%)	196 (90.3%)	181 (83.4%)	96 (44.2%)
Residues in additional allowed regions (a, b, l, p)	15 (15.5%)	17 (7.8%)	29 (13.4%)	80 (36.9%)
Residues in generously allowed regions (~a, ~b, ~l, ~p)	0(0.00%)	3 (1.4%)	5 (2.3%)	25 (11.5%)
Residues in disallowed regions	1(1.0%)	1 (0.5%)	2 (0.9%)	16 (7.4%)
Number of nonglycine and nonproline residues	97	217	217	217
Number of end residues (excl. Gly and Pro)	1	2	2	2

Number of glycine residues (shown as triangles)	7	18	18	18
Number of proline residues	2	10	10	10
Total number of residues	107	247	247	247

Analysis of protein-protein/ Gene-gene interaction

The functional pattern of *BDNF* protein interactions with other proteins, including *MECD2, CTNNBI, NTRK1, NTRK2, NTRK3, NGFR, NTF3, SORT1, NTF4*, and *CPE,* was predicted using the STRING database, revealing strong functional associations (Figure 5A). Studies found that *SORT1* is involved in the endocytosis of progranulin (*PGRN*), a protein significant in frontotemporal lobar degeneration (FTLD-TDP). The intricate link between SORT1 (a neuronal receptor) and *BDNF* emphasizes its role in modulating neurotrophic factor pathways and disease mechanisms, such as Alzheimer's disease and chronic pain (101). The high-affinity receptor *NTRK2* and *BDNF* interact to affect an individual's risk of developing paranoid schizophrenia (102). The findings show the significance *BDNF* plays in a variety of biological processes, such as neuronal differentiation, survival, and development, and the interactions between neurons and other proteins. The significance of *BDNF* signaling anomalies in the etiology of anxiety, cognitive impairment, and Huntington's disease, was also revealed by the GeneMANIA server (103). It determines co-expressed genes, shared protein domains, and functional contributions that contribute to similar biological functions. The gene-gene interaction of the *BDNF* protein was evaluated by the GeneMANIA tool. We got 20 genetic interaction associations (Figure 5B).

The following genes *HAP1, MMP7, CASP6, MMP3, PLG, NGF, MAP2K5, NTF3, NTRK2, DYNLT1, CPE, NTRK2*, and *NTF4* showed co-expressions, and 9 predicted genes such as *SORT1, NGF, NTF3, CPE, NTRK2, GIPC1, NTF4, SORCS2* and *NOS3* were identified. Moreover, 4 co-localized genes were identified including *NTF4, NTRK2, CPE,* and *ZNF274*. The genetic interactions were found in *POU4F3, SORCS2, CPE, MMP7, ADAM17, ZNF274, SORT1, NGF, NTF3, NTRK2, MAP2K5, EHD4, PLG, MMP3* and *CASP6*. The *MMP7, SORCS2, NTF4, NGF, NTF3, SORT1* and *MMP3* share domain and studies identified that genes including NGF, *MAP2K5*, and *NTRK2* were found to co-express, and predicted genes including *GIPC1* and *SORT1* were found. Furthermore, co-domains between *MMP7* and *NTF3* genes were identified, and also with co-localized *NTF4* and *CPE* genes (104, 105). These findings underscore the intricate regulatory mechanisms governing *BDNF* expression and its implications in neuronal function and disease pathogenesis.

Structure-Based Virtual Screening (SBVS)

Molecular docking studies provide important insights into protein-ligand interaction, active compound research, molecular process interpretation, and drug development and design. The Q4L0Y3.1 protein was chosen as the receptor for the docking study and the ligands were a group of compound libraries. PyRx AutoDock VINA was used to calculate the binding energy. A grid box of the proper size was positioned centered on the coordinates of the crystal structure to determine the active site of target protein. PyMOL and Discovery Studio were employed to further evaluate the results of the protein structure predictions and interactions. The top 21 compounds obtained from the PubChem database, whose binding free energies range from -8.5 to -4 Kcal/mol (Figure 6). The identified ligands that target the *BDNF* protein and have high docking scores have potential as drug candidates.

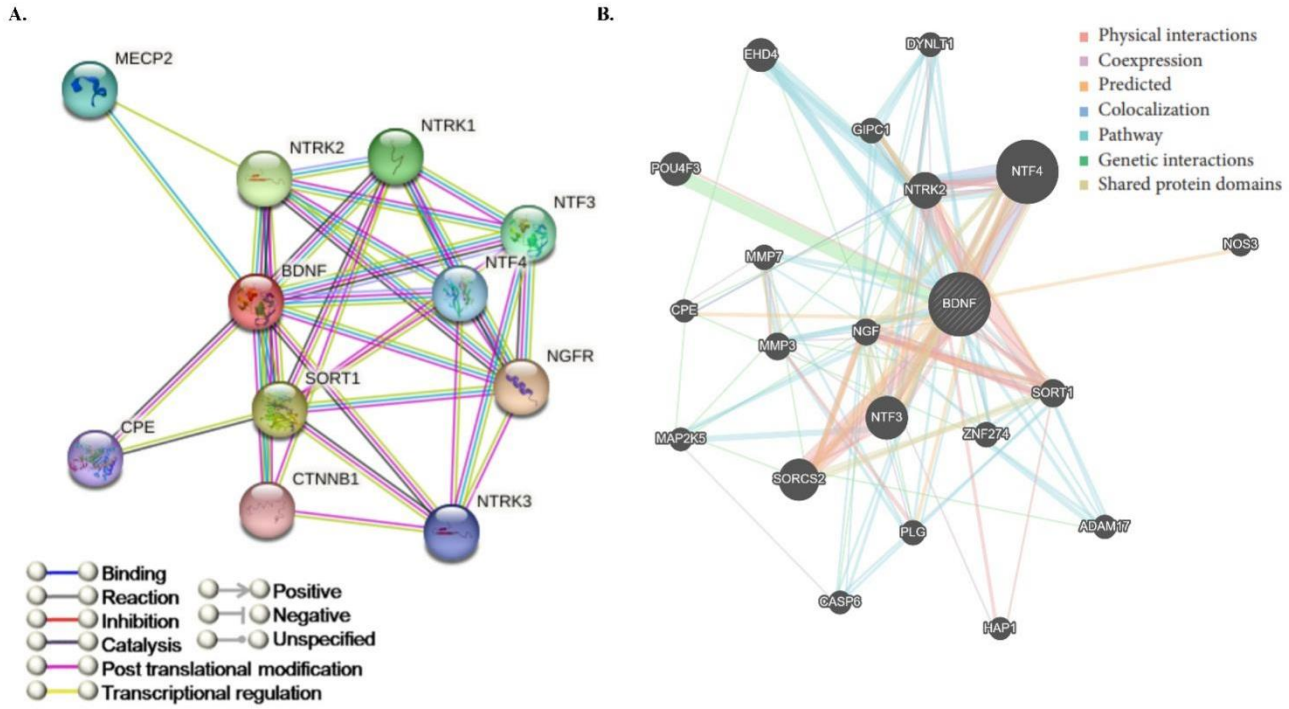

Figure 5: A) The STRING server presents the network of *BDNF*-predicted proteins interacting with the query protein. Colored nodes (query proteins and first shell of interactors), Empty nodes (proteins of unknown 3D structure), and Filled nodes (3D structure is known/predicted). Edges represent protein-protein associations B) GENE MANNIA mediated interactions in the *BDNF*-related genes network.

The complex interaction analysis was conducted using the Ligplot+ program, where non-bonded interactions are represented by spokes, and H-bonds are indicated by dashed green lines, with lengths specified in angstroms (Å). Residues from chain C are depicted with purple bonds, and chain F is represented in orange (Figure 7). The 2D interaction diagram produced by Discovery Studio as a result of ligand atoms interacting with particular residues in the *BDNF* active site (Figure 8). Particularly, interactions between the ligands and the *BDNF* protein are shown in the diagram by the dotted lines.

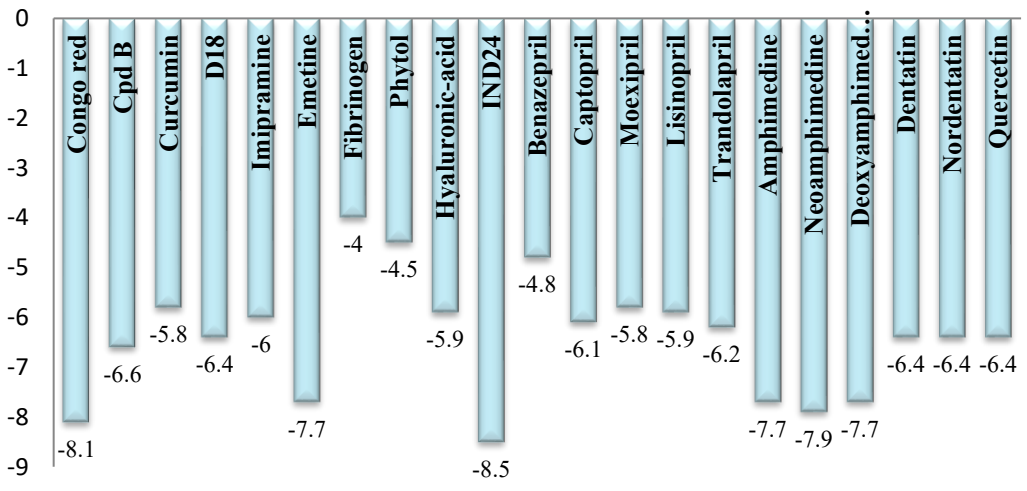

Figure 6: The PyRx program computes the docking score for 21 compounds

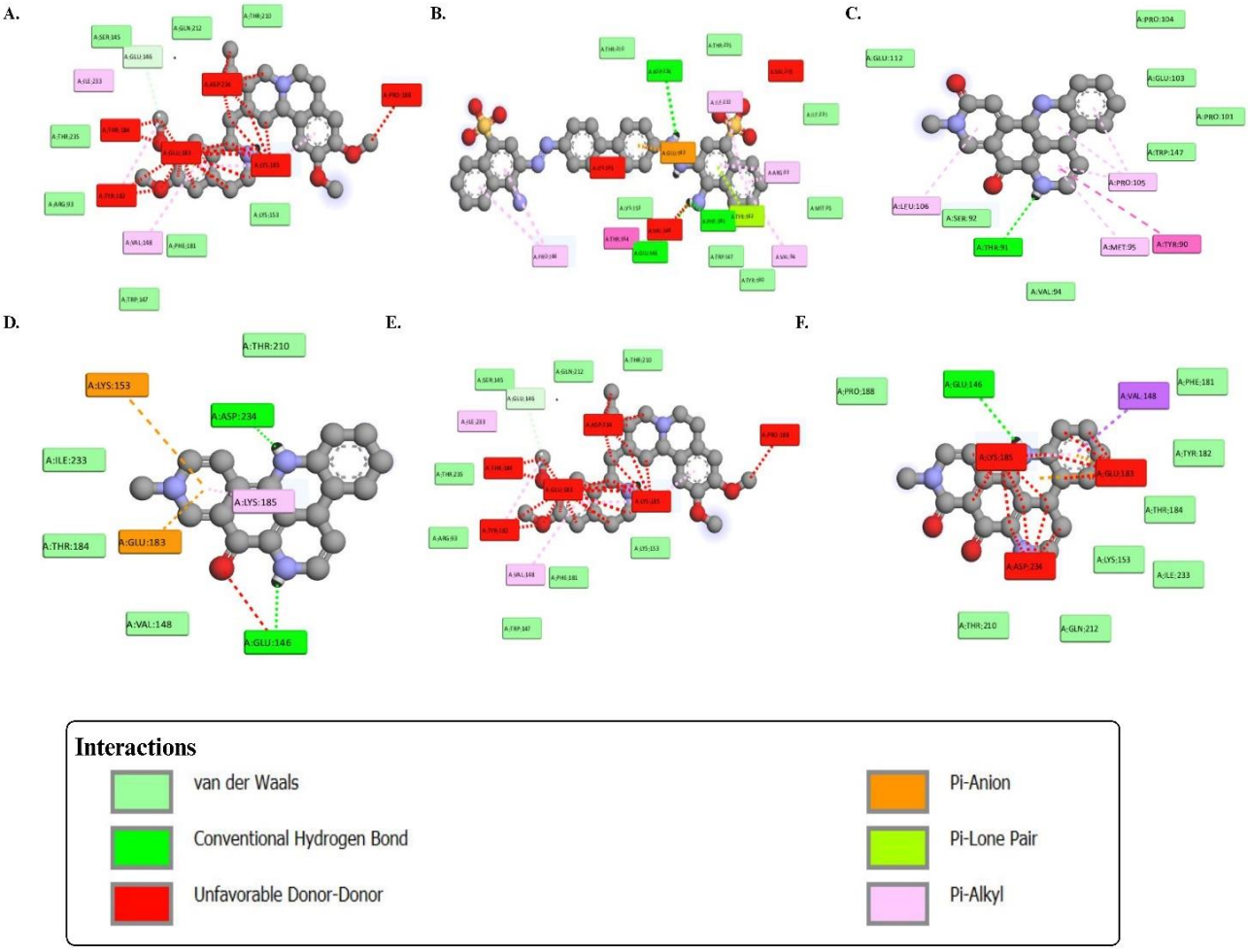

Figure 8: Hydrophilic and Hydrophobic interaction of wild-type *BDNF* protein with IND24, Congo Red, Amphimedine, Deoxyamphimedine, Neoamphimedine, and Emetine

As shown in Figure 7, six ligands with significant binding affinities to the wild-type *BDNF* protein were identified; IND 24, Congo red, Neoamphimedine, Amphimedine, Deoxyamphimedine, and Emetine (from left to right). The binding free energy of all these selected ligands is higher than -4 Kcal/mol, indicating strong potential for effective interaction with the protein. The docking interaction between the *BDNF* protein and the IND24 ligand (Figure 8), predicts several possible binding modes. The ligand forms a carbon-hydrogen bond with GLU146 and exhibits Van der Waals interactions with GLN212, THR210, SER145, LYS153, PHE181, TRP147, ARG93, and THR235. Additionally, IND24 engages in hydrophobic interactions, including Pi-Sigma, Pi-Pi-T-shaped, Alkyl, and Pi-Alkyl, with ILE233 and VAL148. However, it also shows unfavorable interactions with ASP234, LYS148, PRO138, GLU183, TYR182, and THR184. Secondly, Congo Red (CR) exhibits significant potential in modulating amyloid aggregation and neurotoxicity in Alzheimer's disease (AD) by binding site-specifically to amyloid fibrils (106). CR has been found to stabilize amyloid-β monomers, inhibit oligomerization, and impact the binding of acetylcholinesterase to amyloid-β, elucidating its crucial role in influencing the mechanisms underlying neurodegenerative diseases (107).

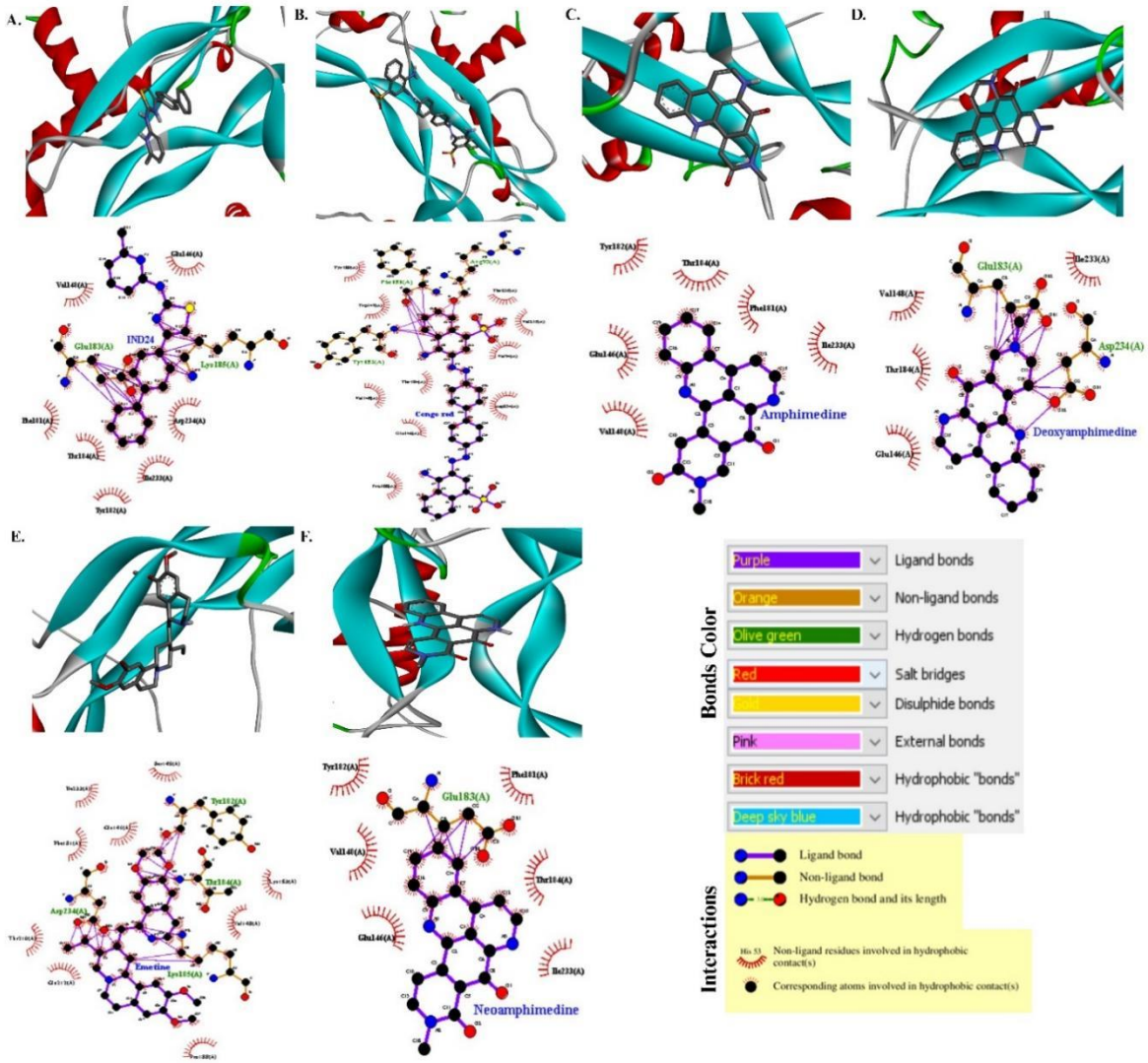

Figure 7: LIGPLOT⁺ representation of intermolecular interactions between the *BDNF* protein and the selected ligands

Such interactions are crucial for understanding the mechanisms underlying neurodegenerative diseases and developing potential therapeutic interventions. The results indicate that Congo Red (CR) interacted with PHE161, GLU146, and ASP234 through conventional hydrogen bonds, and exhibited Vander Waals interactions with THR210, THR235, ILE230, MET95, TRP147, TYR100, and LYS153. Additionally, CR engaged in hydrophobic interactions with GLU113, TYR182, THR184, PRO163, VAL94, ILE231, and ARG93. However, it showed unfavorable bump interactions with VAL245, VAL148, and LYS195 (Figure 7). The study suggests that certain residues, including GLU146, PRO188, THR210, GLN212, THR184, LYS153, TYR188, and PHE181, displayed hydrogen bond interactions with Neoamphimedine (Figure7). These interactions indicate their potential role in stimulating *BDNF* activity. Neoamphimedine (a potent antitumor agent) has shown promise in the treatment of neurological diseases due to its ability to inhibit TopoIIα activity and enhance DNA repair and purinergic pathways. This potential therapeutic value in neurological disease treatment warrants further exploration in preclinical and clinical studies (108, 109).

Furthermore, the compound Amphimedine was observed to interact with the binding pocket of *BDNF* through hydrogen bonds with SER92, VAL94, TRP147, PRO101, GLU103, and PRO104. Moreover, significant hydrophobic interactions were identified with TYR90,

TYR91, PRO105, MET95, and LEU106 (Figure7). Deoxyamphimedine showed interactions forming conventional hydrogen bonds with GLU146 and ASP234 and engaged in Van der Waals interactions with ILE233, THR184, TYR210, and VAL148. It also formed Pi-alkyl interactions with LYS185 and a Pi-cation bond with GLU183 and LYS153 (Figure7). In Figure 8, Emetine establishes hydrophilic interactions with SER145, GLN212, THR210, THR235, TRP147, PHE181, LYS153, ARG93, and PHE151. It also exhibits significant hydrophobic interactions with ILE233, VAL148, THR184, GLU183, TYR182, LYS185, PRO188, and ASP234. Research has shown that Emetine binds significantly to various proteins, including Nsp15, Nsp12, and RdRp, which are essential for viral infection and replication. While its primary interactions have been studied in the viral proteins, examining its interactions with *BDNF* could provide insights into potential effects on glucose metabolism and neuronal activity (110).

Research indicates that PUFA metabolites (LXA_4, NPD1, and HDHA), have a higher affinity for *BDNF* than do PUFAs in their native forms, including omega-3 and omega-6. This indicates that these metabolites could potentially lessen the consequences of type-2 diabetes by binding to *BDNF* and increasing its activity in cognitive performance. LXA_4 showed the greatest affinity for *BDNF* of all the PUFAs that were evaluated (36). Eight ligands were examined in a different study by docking analysis involving citalopram, ampakines, fingolimod phosphate, donepezil, memantine, rasagiline, fluoxetine, and cystamine. Consequently, more in vitro research is necessary to investigate how fingolimod phosphate might lessen the consequences of AD (32, 111). The results of this study highlight the need for more research into the therapeutic potential of the discovered ligands in neurological treatments as it suggests that they may be able to modify the activity of the *BDNF* protein. Further studies, including molecular dynamics simulations, also in vivo and in vitro experiments are necessary to validate these findings comprehensively.

DISCUSSION

The neurological conditions affect more than half of the people in developed countries at some point in their lifespans (12). Abnormal levels of brain-derived neurotrophic factor (*BDNF*) are linked to the development of anxiety, drug dependence, and obsessive-compulsive disorder, all are hallmarks of neuropsychiatric conditions (11). The *BDNF* Val66Met (V66M) mutation may raise the risk of major depressive disease, especially after early-life stress. The exact mechanisms and prevalence rates of multiple neurological diseases associated with *BDNF* variations are still being studied (48). The *BDNF* gene is a complex gene with 9 functional promoters and 11 exons that are found on human chromosome 11p13. Because of this complexity, alternate splicing and promoter use can produce at least 34 distinct transcripts (44, 112). The intra-or extracellular cleavage of pre-pro-BDNF produces different isoforms, including pro-BDNF and mature BDNF (mBDNF) (21, 44). The neurotrophin family encodes *BDNF*, which has a major function in controlling synaptic plasticity, neuronal survival, and neuronal development. It binds to its receptor, tropomyosin-related kinase B (TrkB, also known as Ntrk2), and has remarkable affinity (21, 22).

The primary producers of *BDNF* protein are microglia, astrocytes in the cortex and hippocampus, and glutamatergic neurons (23-25). The biological significance of *BDNF* in many organs is still unknown, even though its effects on the brain are being extensively studied (28, 29). Reduced *BDNF* expression is associated with Huntington's disease, Alzheimer's disease, schizophrenia, and bipolar disorder (30, 31). The *BDNF* is believed to alter synaptic efficacy and induce long-lasting alterations in synaptic plasticity by influencing pre- and post-synaptic regions (32-34). The mutations found in the *BDNF* gene were associated with abnormalities in cellular interactions and dysregulation of gene expression (14, 15). Notably, it is known that missense *BDNF* mutations impact dendritic and neuronal development, causing aberrant growth and early dendritic development (16). There are around 1768 missense variations in the *BDNF* gene known to exist. Multiple studies have

linked the most often identified SNP (rs6265) to cognitive deficits and a decrease in *BDNF* production (17-20). Comprehending protein structure is important to understand the biological functions and the potential structural alterations driven by pathogenic *BDNF* mutations (51, 52). Computational methods are increasingly being used to predict protein 3D structures and identify the probability of genetic mutations.

The present study involved a thorough structural and functional assessment of the *BDNF* protein, with an emphasis on physicochemical parameter identification and homology modeling through the use of bioinformatics tools. The molecular docking study of the *BDNF* gene involved exploring potential interactions between the target protein and various ligands. We aimed to identify binding sites, assess binding affinities, and predict the structural characteristics of the protein-ligand complexes. This knowledge will be useful in confirming the anticipated interactions and exploring any potential therapeutic effects.To comprehend the functional consequences of the human *BDNF* gene, the representative protein sequence (P23560) was obtained from the UniProt dataset. The NCBI database contains significant details about the *BDNF* protein, such as its gene name, length, exon composition, gene ID, data source, and structural information. The physicochemical characteristics of the *BDNF* protein (P23560), as determined by the ProtParam Server, depict it as having a MW of 27,817.94 daltons and an MF of $C_{1211}H_{1950}N_{348}O_{368}S_{17}$. The target protein has an aliphatic index of 74.57 and an instability index (II) of 43.34, indicating that it is unstable. The GRAVY index is -0.456, suggesting that it is hydrophilic and soluble. Using STRING and GeneMANIA tools, the interaction studies show interactions between various biological processes, cellular components, molecular activities, and pathways.

The STRING database was used to predict the functional pattern of *BDNF* interactions with additional proteins, such as *MECD2, CTNNBI, NTRK1, NTRK2, NTRK3, NGFR, NTF3, SORT1, NTF4*, and *CPE*, showing substantial functional interactions. Nine predicted genes were discovered by GENE MAINA, and the following genes had co-expressions; *HAP1, MMP7, CASP6, MMP3, PLG, NGF, MAP2K5, NTF3, NTRK2, DYNLT1, CPE, NTRK2*, and *NTF4*. In addition, *NTF4, NTRK2, CPE*, and *ZNF274* were shown to be co-localized genes. *POU4F3, SORCS2, CPE, MMP7, ADAM17, ZNF274, SORT1, NGF, NTF3, NTRK2, MAP2K5, EHD4, PLG, MMP3*, and *CASP6* all showed genetic connections. The shared domain is occupied by *MMP7, SORCS2, NTF4, NGF, NTF3, SORT1*, and *MMP3*. Research has revealed that co-expressed genes such as *NGF, MAP2K5*, and *NTRK2* were discovered, along with *GIPC1* and *SORT1* genes. Furthermore, co-domains between *MMP7* and *NTF3* genes were identified, and also with co-localized *NTF4* and *CPE* genes (104, 105).

These findings underscore the intricate regulatory mechanisms governing *BDNF* expression and its implications in neuronal function and disease pathogenesis. Understanding the subcellular location and function of proteins depends on the prediction of secondary structures. The SOPMA and PSIPHRED analysis explored the secondary structure composition consisting of α-helix, linker regions, β-sheets, and random strands. This study revealed α-helices were predominant, comprising 34.82% (86 residues), extended strands accounted for 16.19% (40 residues), β-turns represented 7.69% (19 residues), and random coils made up the majority at 41.30% (102 residues). The significant amount of α-helices suggests inherent structural stability and strong thermal endurance of the *BDNF* protein. Moreover, the scarcity of experimentally solved target protein structures makes tertiary structure prediction more difficult. To shed light on the structure and function of proteins, this study attempts to fill the gap between currently accessible protein sequences and experimentally confirmed structures.

The complete structure of the *BDNF* protein is not fully available in the PDB database. To address this gap, *BDNF s*tructures were generated using 4 homology modeling servers; HHPred, i-TASSER, Modeller 10.3, and Swiss-

Model. A template (Q4L0Y3.1.A), representing the crystal structure of a mutant *Spermophilus citellus* protein, was selected for further analysis due to its 97.98% sequence similarity with the *BDNF* query sequence, covering the range of 1-247 amino acids. The validated and refined protein model, characterized by the RAMACHANDRAN plot and model-quality metrics, serves as a basis for subsequent docking analysis. The evaluation metrics of different *BDNF* prediction models are highlighted as follows: HHPred (6XUO_A) exhibits a QMEAN value of -0.77, a ProSA web Z-score of -5.75, and an ERRAT value of 95.699. The Swiss model (Q4L0Y3.1.A) shows a QMEAN value of -2.00, a ProSA web Z-score of -4.96, and an ERRAT value of 90.805. The i-TASSER (model 1) has a QMEAN value of -3.09, a ProSA web Z-score of -1.96, and an ERRAT value of 82.077. Modeller 10.3 (bdnf.B99990010) demonstrates a QMEAN value of -6.20, a ProSA web Z-score of -3.23, and an ERRAT value of 34.310. These metrics are crucial for assessing the quality and reliability of the selected structure predictions.

The study utilizes protein-ligand docking analysis, employing the PyRx program, to simulate interactions between the *BDNF* protein and selected compounds. Twenty-one compounds were obtained from the PubChem database, with binding free energies ranging from -8.5 to -4 Kcal/mol. Among these, IND 24, Congo red, Neoamphimedine, Amphimedine, Deoxyamphimedine, and Emetine were chosen for further study based on their high binding energies. Docking studies revealed potential binding mechanisms, key amino acid residues involved in interactions, and the overall complex stability between these ligands and the *BDNF* protein. These findings may have significant consequences for therapeutic research, drug discovery, and our understanding of *BDNF*-related diseases. Discovery Studio and LIGPLOT^{+} enable the visualization of complex interactions by providing a 2D or 3D perspective on non-bonded and hydrogen bond interactions between ligands and the *BDNF* protein. This study emphasizes the utility of bioinformatics methods in exploring the therapeutic potential of the *BDNF* gene and demands further investigation into its implications for disease and drug discovery. Bioinformatics provides a cost-effective approach to rapidly analyze the expected impacts of genetic variants, but improving prediction accuracy requires considering additional variables. Ultimately, validating these computational findings through clinical wet lab studies is essential. This process will enable the translation of insights into actionable knowledge, facilitating the development of therapeutic interventions targeting the *BDNF* gene and its associated pathways.

CONCLUSION

The neurotrophin *BDNF* protein is well-known for its function in the central nervous system (CNS) and is implicated in numerous neurological diseases. To date, a total of 1768 missense mutations have been identified in the *BDNF* gene. Regulation of *BDNF* protein levels is crucial for synaptic function, cell survival, and its effective secretion and transport mechanisms. This study endeavors to present structural and functional annotations of the protein using computational methods. The findings suggest that the chosen protein is a viable target for protein-ligand docking to develop putative therapeutic compounds. Physicochemical analysis characterized P23560 as a protein that is negatively charged, basic in nature, and unstable. Network analysis underscores the intricate regulatory mechanisms leading to *BDNF* expression and its implications in neuronal function and disease pathogenesis. Structural predictions revealed that α-helices were more predominant than β-sheets within the *BDNF* protein. The 3D structure was generated for homology modeling using the SwissModel server, and the model quality was confirmed using QMEAN, ProSA, and SAVES analysis. The LigPlot^{+} tool and Discovery Studio were used to examine possible interactions between the selected ligands and the target protein. The interactions with discovered ligands with favorable binding energies show promise for potential treatments for *BDN*F-driven disease. Moreover, researchers aim to discover new therapeutic candidates that can modulate the function of the selected protein and potentially

impact associated brain diseases. Understanding these molecular interactions is crucial for investigating their biological consequences.

REFERENCES

1. Dakal TC, Kala D, Dhiman G, Yadav V, Krokhotin A, Dokholyan NV. Predicting the functional consequences of non-synonymous single nucleotide polymorphisms in IL8 gene. Scientific reports. 2017;7(1):6525.
2. Zou H, Wu L-X, Tan L, Shang F-F, Zhou H-H. Significance of single-nucleotide variants in long intergenic non-protein coding RNAs. Frontiers in Cell and Developmental Biology. 2020;8:347.
3. Spencer DH, Zhang B, Pfeifer J. Single nucleotide variant detection using next generation sequencing. Clinical genomics: Elsevier; 2015. p. 109-27.
4. Samir S. Human DNA Mutations and their Impact on Genetic Disorders. Recent Patents on Biotechnology. 2024;18(4):288-315.
5. Zou H, Wu LX, Tan L, Shang FF, Zhou HH. Significance of Single-Nucleotide Variants in Long Intergenic Non-protein Coding RNAs. Front Cell Dev Biol. 2020;8:347.
6. Xu D, Shao Q, Zhou C, Mahmood A, Zhang J. In silico analysis of nsSNPs of human KRAS gene and protein modeling using bioinformatic tools. ACS omega. 2023;8(14):13362-70.
7. Cargill M, Altshuler D, Ireland J, Sklar P, Ardlie K, Patil N, et al. Characterization of single-nucleotide polymorphisms in coding regions of human genes. Nature genetics. 1999;22(3):231-8.
8. Bhat GR, Sethi I, Rah B, Kumar R, Afroze D. Innovative in Silico Approaches for Characterization of Genes and Proteins. Frontiers in Genetics. 2022;13:865182.
9. Saikat ASM, Paul AK, Dey D, Das RC, Das MC. In-Silico Approaches for Molecular Characterization and Structure-Based Functional Annotation of the Matrix Protein from Nipah henipavirus. Chemistry Proceedings. 2022;12(1):21.
10. Sahay A, Piprodhe A, Pise M. In silico analysis and homology modeling of strictosidine synthase involved in alkaloid biosynthesis in catharanthus roseus. Journal of Genetic Engineering and Biotechnology. 2020;18:1-6.
11. De Oliveira CCS, Pereira GRC, De Alcantara JYS, Antunes D, Caffarena ER, De Mesquita JF. In silico analysis of the V66M variant of human BDNF in psychiatric disorders: An approach to precision medicine. Plos one. 2019;14(4):e0215508.
12. Trautmann S, Wittchen H-u. Do our societies react appropriately to the burden of mental disorders. EMBO reports. 2016;17(9):1245-9.
13. Cattaneo A, Cattane N, Begni V, Pariante CM, Riva M. The human BDNF gene: peripheral gene expression and protein levels as biomarkers for psychiatric disorders. Translational psychiatry. 2016;6(11):e958-e.
14. Nestor PG, O'Donovan K, Lapp HE, Hasler VC, Boodai SB, Hunter R. Risk and protective effects of serotonin and BDNF genes on stress-related adult psychiatric symptoms. Neurobiology of stress. 2019;11:100186.
15. Devlin P, Cao X, Stanfill AG. Genotype-expression interactions for BDNF across human brain regions. BMC genomics. 2021;22:1-11.
16. Deacon BJ. The biomedical model of mental disorder: A critical analysis of its validity, utility, and effects on psychotherapy research. Clinical psychology review. 2013;33(7):846-61.
17. Narayanan V, Veeramuthu V, Ahmad-Annuar A, Ramli N, Waran V, Chinna K, et al. Missense mutation of brain derived neurotrophic factor (BDNF) alters neurocognitive performance in patients with mild traumatic brain injury: a longitudinal study. PLoS One. 2016;11(7):e0158838.
18. Chen Z-Y, Patel PD, Sant G, Meng C-X, Teng KK, Hempstead BL, et al. Variant brain-derived neurotrophic factor (BDNF)(Met66) alters the intracellular trafficking and activity-dependent secretion of wild-type BDNF in neurosecretory cells and cortical neurons. Journal of Neuroscience. 2004;24(18):4401-11.
19. Dincheva I, Glatt CE, Lee FS. Impact of the BDNF Val66Met polymorphism on cognition: implications for behavioral genetics. The Neuroscientist. 2012;18(5):439-51.
20. Fatma R, Chauhan W, Shahi MH, Afzal M. Association of BDNF gene missense polymorphism rs6265 (Val66Met) with three quantitative traits, namely, intelligence quotient, body mass index, and blood pressure: a genetic association analysis from North India. Frontiers in Neurology. 2022;13.
21. Colucci-D'Amato L, Speranza L, Volpicelli F. Neurotrophic factor BDNF, physiological functions and therapeutic potential in depression, neurodegeneration and brain cancer. International journal of molecular sciences. 2020;21(20):7777.
22. Tettamanti G, Cattaneo AG, Gornati R, de Eguileor M, Bernardini G, Binelli G. Phylogenesis of brain-derived neurotrophic factor (BDNF) in vertebrates. Gene. 2010;450(1-2):85-93.
23. Andreska T, Aufmkolk S, Sauer M, Blum R. High abundance of BDNF within glutamatergic

presynapses of cultured hippocampal neurons. Frontiers in cellular neuroscience. 2014;8:107.
24. Clarke LE, Liddelow SA, Chakraborty C, Münch AE, Heiman M, Barres BA. Normal aging induces A1-like astrocyte reactivity. Proceedings of the National Academy of Sciences. 2018;115(8):E1896-E905.
25. Parkhurst CN, Yang G, Ninan I, Savas JN, Yates JR, Lafaille JJ, et al. Microglia promote learning-dependent synapse formation through brain-derived neurotrophic factor. Cell. 2013;155(7):1596-609.
26. Hennigan A, O'callaghan R, Kelly A. Neurotrophins and their receptors: roles in plasticity, neurodegeneration and neuroprotection. Portland Press Ltd.; 2007.
27. Rosenberg SS, Ng BK, Chan JR. The quest for remyelination: a new role for neurotrophins and their receptors. Brain pathology. 2006;16(4):288-94.
28. Huang EJ, Reichardt LF. Neurotrophins: roles in neuronal development and function. Annual review of neuroscience. 2001;24(1):677-736.
29. Iu ECY, Chan CB. Is Brain-Derived Neurotrophic Factor a Metabolic Hormone in Peripheral Tissues? Biology. 2022;11(7):1063.
30. Marosi K, Mattson MP. BDNF mediates adaptive brain and body responses to energetic challenges. Trends in Endocrinology & Metabolism. 2014;25(2):89-98.
31. Mehterov N, Minchev D, Gevezova M, Sarafian V, Maes M. Interactions among brain-derived neurotrophic factor and neuroimmune pathways are key components of the major psychiatric disorders. Molecular Neurobiology. 2022;59(8):4926-52.
32. Mahendran R, Jeyabasker S, Francis A, Manoharan S. Homology Modeling and in silico docking analysis of BDNF in the treatment of Alzheimer's disease. Research Journal of Pharmacy and Technology. 2017;10(9):2899-906.
33. Itami C, Kimura F, Kohno T, Matsuoka M, Ichikawa M, Tsumoto T, et al. Brain-derived neurotrophic factor-dependent unmasking of “silent” synapses in the developing mouse barrel cortex. Proceedings of the National Academy of Sciences. 2003;100(22):13069-74.
34. Edelmann E, Leßmann V, Brigadski T. Pre-and postsynaptic twists in BDNF secretion and action in synaptic plasticity. Neuropharmacology. 2014;76:610-27.
35. Krabbe K, Nielsen A, Krogh-Madsen R, Plomgaard P, Rasmussen P, Erikstrup C, et al. Brain-derived neurotrophic factor (BDNF) and type 2 diabetes. Diabetologia. 2007;50:431-8.
36. Kumar YP, Srinivas GSS, Malla L, Rao AA. Agonistic approach of omega-3, omega-6 and its metabolites with BDNF: An In-silico study. Bioinformation. 2013;9(18):908.
37. Wheeler DL, Barrett T, Benson DA, Bryant SH, Canese K, Church DM, et al. Database resources of the national center for biotechnology information. Nucleic acids research. 2005;33(suppl_1):D39-D45.
38. Li G, Zhang J, Guo Q, Wei J, Jiang Y, Zhao X, et al. Study of efflux pump gene expression in rifampicin-monoresistant Mycobacterium tuberculosis clinical isolates. The Journal of antibiotics. 2015;68(7):431-5.
39. Miranda M, Morici JF, Zanoni MB, Bekinschtein P. Brain-derived neurotrophic factor: a key molecule for memory in the healthy and the pathological brain. Frontiers in cellular neuroscience. 2019:363.
40. Losenkov IS, Mulder NJ, Levchuk LA, Vyalova NM, Loonen AJ, Bosker FJ, et al. Association between BDNF gene variant Rs6265 and the severity of depression in antidepressant treatment-free depressed patients. Frontiers in psychiatry. 2020;11:38.
41. Bothwell M. Functional interactions of neurotrophins and neurotrophin receptors. Annual review of neuroscience. 1995;18(1):223-53.
42. Klein R, Conway D, Parada LF, Barbacid M. The trkB tyrosine protein kinase gene codes for a second neurogenic receptor that lacks the catalytic kinase domain. Cell. 1990;61(4):647-56.
43. Klein R, Nanduri V, Jing S, Lamballe F, Tapley P, Bryant S, et al. The trkB tyrosine protein kinase is a receptor for brain-derived neurotrophic factor and neurotrophin-3. Cell. 1991;66(2):395-403.
44. Bathina S, Das UN. Brain-derived neurotrophic factor and its clinical implications. Archives of medical science. 2015;11(6):1164-78.
45. Kowiański P, Lietzau G, Czuba E, Waśkow M, Steliga A, Moryś J. BDNF: a key factor with multipotent impact on brain signaling and synaptic plasticity. Cellular and molecular neurobiology. 2018;38:579-93.
46. Serra-Millàs M. Are the changes in the peripheral brain-derived neurotrophic factor levels due to platelet activation? World journal of psychiatry. 2016;6(1):84.
47. Lessmann V, Gottmann K, Malcangio M. Neurotrophin secretion: current facts and future prospects. Progress in neurobiology. 2003;69(5):341-74.
48. Autry AE, Monteggia LM. Brain-derived neurotrophic factor and neuropsychiatric disorders. Pharmacological reviews. 2012;64(2):238-58.
49. Pruunsild P, Kazantseva A, Aid T, Palm K, Timmusk T. Dissecting the human BDNF locus:

bidirectional transcription, complex splicing, and multiple promoters. Genomics. 2007;90(3):397-406.
50. Numakawa T, Suzuki S, Kumamaru E, Adachi N, Richards M, Kunugi H. BDNF function and intracellular signaling in neurons. Histology and histopathology. 2010.
51. Dorn M, e Silva MB, Buriol LS, Lamb LC. Three-dimensional protein structure prediction: Methods and computational strategies. Computational biology and chemistry. 2014;53:251-76.
52. Zhou H, Gao M, Skolnick J. ENTPRISE: an algorithm for predicting human disease-associated amino acid substitutions from sequence entropy and predicted protein structures. PLOS one. 2016;11(3):e0150965.
53. Krebs BB, De Mesquita JF. Amyotrophic lateral sclerosis type 20-In Silico analysis and molecular dynamics simulation of hnRNPA1. PloS one. 2016;11(7):e0158939.
54. Gao M, Zhou H, Skolnick J. Insights into disease-associated mutations in the human proteome through protein structural analysis. Structure. 2015;23(7):1362-9.
55. Hassan MO, Gassim DA, Albakrye AM, Elnasri HA, Khaier MA. In silico analysis of likely pathogenic variants in human GGCX gene. Informatics in Medicine Unlocked. 2020;19:100337.
56. Rozario LT, Sharker T, Nila TA. In silico analysis of deleterious SNPs of human MTUS1 gene and their impacts on subsequent protein structure and function. Plos One. 2021;16(6):e0252932.
57. Kouranov A, Xie L, de la Cruz J, Chen L, Westbrook J, Bourne PE, et al. The RCSB PDB information portal for structural genomics. Nucleic acids research. 2006;34(suppl_1):D302-D5.
58. Wilkins MR. Protein identification and analysis tools in the ExPASy server. Methods Mol Biol. 1999;112:531.
59. Gasteiger E, Hoogland C, Gattiker A, Duvaud Se, Wilkins MR, Appel RD, et al. Protein identification and analysis tools on the ExPASy server: Springer; 2005.
60. Geourjon C, Deleage G. SOPMA: significant improvements in protein secondary structure prediction by consensus prediction from multiple alignments. Bioinformatics. 1995;11(6):681-4.
61. Angamuthu K, Piramanayagam S. Evaluation of in silico protein secondary structure prediction methods by employing statistical techniques. Biomedical and Biotechnology Research Journal (BBRJ). 2017;1(1):29.
62. Altschul SF, Madden TL, Schäffer AA, Zhang J, Zhang Z, Miller W, et al. Gapped BLAST and PSI-BLAST: a new generation of protein database search programs. Nucleic acids research. 1997;25(17):3389-402.
63. Mustafa MI, Murshed NS, Abdelmoneim AH, Makhawi AM. In silico analysis of the functional and structural consequences of SNPs in human ARX gene associated with EIEE1. Informatics in Medicine Unlocked. 2020;21:100447.
64. Nailwal M, Chauhan JB. Analysis of consequences of non-synonymous SNPs of USP9Y gene in human using bioinformatics tools. Meta Gene. 2017;12:13-7.
65. Pramanik K, Ghosh PK, Ray S, Sarkar A, Mitra S, Maiti TK. An in silico structural, functional and phylogenetic analysis with three dimensional protein modeling of alkaline phosphatase enzyme of Pseudomonas aeruginosa. Journal of Genetic Engineering and Biotechnology. 2017;15(2):527-37.
66. Buchan DW, Minneci F, Nugent TC, Bryson K, Jones DT. Scalable web services for the PSIPRED Protein Analysis Workbench. Nucleic acids research. 2013;41(W1):W349-W57.
67. Szklarczyk D, Franceschini A, Wyder S, Forslund K, Heller D, Huerta-Cepas J, et al. STRING v10: protein–protein interaction networks, integrated over the tree of life. Nucleic acids research. 2015;43(D1):D447-D52.
68. Ahmad HI, Afzal G, Jamal A, Kiran S, Khan MA, Mehmood K, et al. In silico structural, functional, and phylogenetic analysis of cytochrome (CYPD) protein family. BioMed Research International. 2021;2021:1-13.
69. Raimundo S, Toscano C, Klein K, Fischer J, Griese EU, Eichelbaum M, et al. A novel intronic mutation, 2988G> A, with high predictivity for impaired dunction of cytochrome P450 2D6 in white subjects. Clinical Pharmacology & Therapeutics. 2004;76(2):128-38.
70. Warde-Farley D, Donaldson SL, Comes O, Zuberi K, Badrawi R, Chao P, et al. The GeneMANIA prediction server: biological network integration for gene prioritization and predicting gene function. Nucleic acids research. 2010;38(suppl_2):W214-W20.
71. Laskowski RA, MacArthur MW, Moss DS, Thornton JM. PROCHECK: a program to check the stereochemical quality of protein structures. Journal of applied crystallography. 1993;26(2):283-91.
72. Fiser A, Šali A. Modeller: generation and refinement of homology-based protein structure models. Methods in enzymology. 374: Elsevier; 2003. p. 461-91.
73. Söding J, Biegert A, Lupas AN. The HHpred interactive server for protein homology detection and structure prediction. Nucleic acids research. 2005;33(suppl_2):W244-W8.

74. Colovos C, Yeates TO. Verification of protein structures: patterns of nonbonded atomic interactions. Protein science. 1993;2(9):1511-9.
75. Biegert A, Mayer C, Remmert M, Söding J, Lupas AN. The MPI Bioinformatics Toolkit for protein sequence analysis. Nucleic acids research. 2006;34(suppl_2):W335-W9.
76. Goswami AM. Structural modeling and in silico analysis of non-synonymous single nucleotide polymorphisms of human 3β-hydroxysteroid dehydrogenase type 2. Meta gene. 2015;5:162-72.
77. Gabler F, Nam SZ, Till S, Mirdita M, Steinegger M, Söding J, et al. Protein sequence analysis using the MPI bioinformatics toolkit. Current Protocols in Bioinformatics. 2020;72(1):e108.
78. Hasnain MJU, Shoaib M, Qadri S, Afzal B, Anwar T, Abbas SH, et al. Computational analysis of functional single nucleotide polymorphisms associated with SLC26A4 gene. PLoS One. 2020;15(1):e0225368.
79. Lavadié-González CE, Serrat-Díaz MdJ, Azcanio-Fuentes L. Homology modelling and in silico Structural characterization of lanosterol 14α-demethylase from Cryptococcus neoformans var. Grubii. Revista Cubana de Química. 2021;33(2):198-226.
80. Webb B, Sali A. Comparative protein structure modeling using MODELLER. Current protocols in bioinformatics. 2016;54(1):5.6. 1-5.6. 37.
81. Guex N, Peitsch MC. SWISS-MODEL and the Swiss-Pdb Viewer: an environment for comparative protein modeling. electrophoresis. 1997;18(15):2714-23.
82. Wang S, Li W, Liu S, Xu J. RaptorX-Property: a web server for protein structure property prediction. Nucleic acids research. 2016;44(W1):W430-W5.
83. Yang J, Yan R, Roy A, Xu D, Poisson J, Zhang Y. The I-TASSER Suite: protein structure and function prediction. Nature methods. 2015;12(1):7-8.
84. Zhou X, Zheng W, Li Y, Pearce R, Zhang C, Bell EW, et al. I-TASSER-MTD: a deep-learning-based platform for multi-domain protein structure and function prediction. Nature Protocols. 2022;17(10):2326-53.
85. Pettersen EF, Goddard TD, Huang CC, Couch GS, Greenblatt DM, Meng EC, et al. UCSF Chimera—a visualization system for exploratory research and analysis. Journal of computational chemistry. 2004;25(13):1605-12.
86. Schrödinger L. The PyMOL molecular graphics system, version 1.8. November; 2015.
87. Mahmud Z, Malik SUF, Ahmed J, Azad AK. Computational analysis of damaging single-nucleotide polymorphisms and their structural and functional impact on the insulin receptor. BioMed research international. 2016;2016.
88. Pereira GRC, Da Silva A, Do Nascimento S, De Mesquita J. In silico analysis and molecular dynamics simulation of human superoxide dismutase 3 (SOD3) genetic variants. Journal of cellular biochemistry. 2019;120(3):3583-98.
89. Prajapat R, Marwal A, Gaur R. Recognition of errors in the refinement and validation of three-dimensional structures of AC1 proteins of begomovirus strains by using ProSA-Web. Journal of Viruses. 2014;2014.
90. Khan Y, Ekka MK, Meena LS. Structural and functional characterization of mycobacterial PhoH2 and identification of potential inhibitor of its enzymatic activity. Brazilian Journal of Microbiology. 2024:1-19.
91. Bajorath J. Integration of virtual and high-throughput screening. Nature Reviews Drug Discovery. 2002;1(11):882-94.
92. Jorgensen WL. The many roles of computation in drug discovery. Science. 2004;303(5665):1813-8.
93. Kuntz ID, Blaney JM, Oatley SJ, Langridge R, Ferrin TE. A geometric approach to macromolecule-ligand interactions. Journal of molecular biology. 1982;161(2):269-88.
94. Kalyaanamoorthy S, Chen Y-PP. Structure-based drug design to augment hit discovery. Drug discovery today. 2011;16(17-18):831-9.
95. Inc C. Molecular operating environment (MOE). Chemical Computing Group Inc. 2016;1010.
96. Dallakyan S, Olson AJ. Small-molecule library screening by docking with PyRx. Chemical biology: Springer; 2015. p. 243-50.
97. Morris GM, Huey R, Olson AJ. Using autodock for ligand-receptor docking. Current protocols in bioinformatics. 2008;24(1):8.14. 1-8.. 40.
98. Trott O, Olson AJ. AutoDock Vina: improving the speed and accuracy of docking with a new scoring function, efficient optimization, and multithreading. Journal of computational chemistry. 2010;31(2):455-61.
99. Ferrari IV, Patrizio P. Development and Validation Molecular Docking Analysis of Human serum albumin (HSA). bioRxiv. 2021.
100. Adeniji SE, Uba S, Uzairu A. In silico study for evaluating the binding mode and interaction of 1, 2, 4-triazole and its derivatives as potent inhibitors against Lipoate protein B (LipB). Journal of King Saud University-Science. 2020;32(1):475-85.
101. Belbin O, Morgan K, Medway C, Warden D, Cortina-Borja M, van Duijn CM, et al. The Epistasis Project: A multi-cohort study of the effects of BDNF, DBH, and SORT1 epistasis on Alzheimer's disease

risk. Journal of Alzheimer's Disease. 2019;68(4):1535-47.
102. Lin Z, Su Y, Zhang C, Xing M, Ding W, Liao L, et al. The interaction of BDNF and NTRK2 gene increases the susceptibility of paranoid schizophrenia. PLoS One. 2013;8(9):e74264.
103. Lu B, Nagappan G, Lu Y. BDNF and synaptic plasticity, cognitive function, and dysfunction. Neurotrophic factors. 2014:223-50.
104. Fatma R, Chauhan W, Shahi MH, Afzal M. Association of BDNF gene missense polymorphism rs6265 (Val66Met) with three quantitative traits, namely, intelligence quotient, body mass index, and blood pressure: A genetic association analysis from North India. Frontiers in Neurology. 2023;13:1035885.
105. Esvald E-E, Tuvikene J, Moistus A, Rannaste K, Kõomägi S, Timmusk T. Differential regulation of the BDNF gene in cortical and hippocampal neurons. Journal of Neuroscience. 2022;42(49):9110-28.
106. Li Qy, Yu X, Li X, Bao Ln, Zhang Y, Wang Sl, et al. Congo Red-Derived Carbon Dots: Simultaneously as Fluorescence Probe for Protein Aggregates, Inhibitor for Protein Aggregation, and Scavenger of Free Radicals. Small. 2023;19(18):2205634.
107. Kasai T, Wada T, Iijima T, Minami Y, Sakaguchi T, Koga R, et al. Comparative study of the hydrophobic interaction effect of pH and ionic strength on aggregation/emulsification of Congo red and amyloid fibrillation of insulin. BBA advances. 2022;2:100036.
108. Xu W, Gao L, Li T, Shao A, Zhang J. Neuroprotective role of agmatine in neurological diseases. Current neuropharmacology. 2018;16(9):1296-305.
109. Ponder J, Yoo BH, Abraham AD, Li Q, Ashley AK, Amerin CL, et al. Neoamphimedine circumvents metnase-enhanced DNA topoisomerase IIα activity through ATP-competitive inhibition. Marine Drugs. 2011;9(11):2397-408.
110. Khandelwal N, Chander Y, Rawat KD, Riyesh T, Nishanth C, Sharma S, et al. Emetine inhibits replication of RNA and DNA viruses without generating drug-resistant virus variants. Antiviral research. 2017;144:196-204.
111. Doi Y, Takeuchi H, Horiuchi H, Hanyu T, Kawanokuchi J, Jin S, et al. Fingolimod phosphate attenuates oligomeric amyloid β–induced neurotoxicity via increased brain-derived neurotrophic factor expression in neurons. PloS one. 2013;8(4):e61988.
112. Cattaneo A, Cattane N, Begni V, Pariante C, Riva M. The human BDNF gene: peripheral gene expression and protein levels as biomarkers for psychiatric disorders. Translational psychiatry. 2016;6(11):e958-e.